Open access • Journal Article • DOI:10.1029/2020JD032681

A 4.5 Year-Long Record of Svalbard Water Vapor Isotopic Composition Documents Winter Air Mass Origin — Source link

C. Leroy-Dos Santos, Valérie Masson-Delmotte, Mathieu Casado, Elise Fourré ...+8 more authors

Institutions: Centre national de la recherche scientifique, Geophysical Institute, University of Bergen

Published on: 16 Dec 2020 - Journal of Geophysical Research (John Wiley & Sons, Ltd)

Topics: Air mass, Water vapor, Humidity and Snow

A 4.5 Year-Long Record of Svalbard Water Vapor Isotopic Composition Documents Winter Air Mass Origin

C. Leroy-dos Santos, V. Masson-delmotte, M. Casado, E. Fourré, H. Steen-larsen, M. Maturilli, A. Orsi, A. Berchet, O. Cattani, B. Minster, et al.

A 4.5 year-long record of Svalbard water vapor isotopic composition documents winter air mass origin

C. Leroy-Dos Santos[1], V. Masson-Delmotte[1], M. Casado[2], E. Fourré[1], H. C. Steen-Larsen[3], M. Maturilli[4], A. Orsi[1], A. Berchet[1], O. Cattani[1], B. Minster[1], J. Gherardi[1], A. Landais[1]

[1]Laboratoire des Sciences du Climat et de l'Environnement, UMR CEA-CNRS-UVSQ/IPSL, Gif-sur-Yvette, France.
[2]Alfred Wegener Institute Helmholtz-Center for Polar and Marine Research Bremerhaven, Bremerhaven, Germany.
[3]Geophysical Institute, University of Bergen, Bergen, Norway.
[4]Alfred Wegener Institute Helmholtz-Center for Polar and Marine Research, Potsdam, Germany.

Corresponding author: Christophe Leroy-Dos Santos (christophe.leroy-dos-santos@lsce.ipsl.fr)

Key Points:

- Svalbard is a key location to study the hydrological cycle and long-range moisture transport in the Arctic.
- 4.5 years continuous record of water vapor and precipitation isotopic composition at Ny-Ålesund.
- New isotopic diagnostic to document the origin of air masses at Svalbard.

Abstract

From May 2014 to September 2018, a laser spectrometer analyzer provided a 4.5 years continuous record of water vapor isotopic composition at Ny-Ålesund (8 m a.s.l.), Svalbard. It corresponds to the longest dataset published in polar regions. A comparison of this dataset with a parallel similar dataset obtained during 20 days by a second laser spectrometer installed at the near Mount Zeppelin (474 m a.s.l.) shows that this dataset is representative of a regional signal. In addition, the observation of insignificant diurnal cycles in the isotopic signal compared to the strong isotopic signature of synoptic events and the comparison of simultaneous measurements in the vapor and in rain or snow samples lead to the conclusion that our record reflects a large part of the regional dynamics of the atmospheric water cycle driven by large scale variability. This study focuses on winters dominated by the occurrence of synoptic events associated with humidity peaks. Using statistics and back-trajectories calculations, we link high humidity peaks characterized by an anti-correlation between $\delta^{18}O$ and d-excess in the water vapor to a rapid shift of air mass source regions from the Arctic to the North Atlantic Ocean below 60°N. On the other hand, correlation between $\delta^{18}O$ and d-excess may be associated with a shift of air mass sources within the Arctic. These results demonstrate the added value of long-term water vapor isotopic monitoring to better understand the moisture origin in the Arctic and the atmospheric dynamics.

1. Introduction

In the current context of climate change, the Arctic region is specifically under focus because of the extreme high temperatures and low sea ice extents observed over recent years (Arctic Monitoring and Assessment Programme, 2017; Meredith et al., 2019; Overland & Wang, 2018; Walsh et al., 2017). The long-term increase in annual temperature in the Arctic region is 2-3 times larger than the global average (Gjelten et al., 2016), due to a number of polar amplification processes involving changes in albedo, water vapor, summer cloudiness, the presence of open water in autumn, but also the transport of heat and moisture associated with the intrusion of sub-arctic storms (Goosse et al., 2018; Meredith et al., 2019; Screen & Simmonds, 2010). Linked to atmospheric circulation patterns, recent studies also highlighted the occurrence of "atmospheric rivers" as an important modulation of the moisture transport to the Arctic region (Alekseev et al., 2019; Bonne et al., 2015; Hao et al., 2019; Liu & Barnes, 2015; Naakka et al., 2019; Woods et al., 2013).

Seasonally surrounded by sea ice, Svalbard stands at the intersection between cold polar air travelling from the north and oceanic air travelling from the south (Figure 1). Svalbard is hence at a key location to study changes of the atmospheric water cycle organization in the Arctic region, which is key to gain a better understanding of the role of sea ice extent variations on the Arctic climate processes (Ding et al., 2017) since recent sea ice decline leads to an increase of local evaporation sources (Dufour et al., 2016). Due to its geographic position, Svalbard climate evolution is strongly affected by Arctic amplification (warming at a rate of 0.8 ± 0.2 °C.decade^{-1} on the 1979-2019 period (Figure S1 and Text S1) and is influenced by regional processes controlling sea ice variations and moisture transport from the North Atlantic sector (Dahlke et al., 2020; Hanssen-Bauer & Førland, 1998; Isaksen et al., 2016; Rinke et al., 2017).

A robust signal in climate projections is the increasing trend of Arctic precipitation by the end of the 21st century, but climate models show a large dispersion in the relative contributions of local recycling and enhanced advection to this increase in precipitation amount (Bintanja & Selten, 2014). Two main effects are expected to influence the moisture content in the Svalbard region: evaporation over the ocean (Dufour et al., 2016) and atmospheric circulation patterns leading to moisture transport from Atlantic, Arctic or continental regions (Dahlke & Maturilli, 2017; Vázquez et al., 2016). This motivates the exploration of the air mass origin signal captured by water stable isotopes in Svalbard water vapor and precipitation in this study.

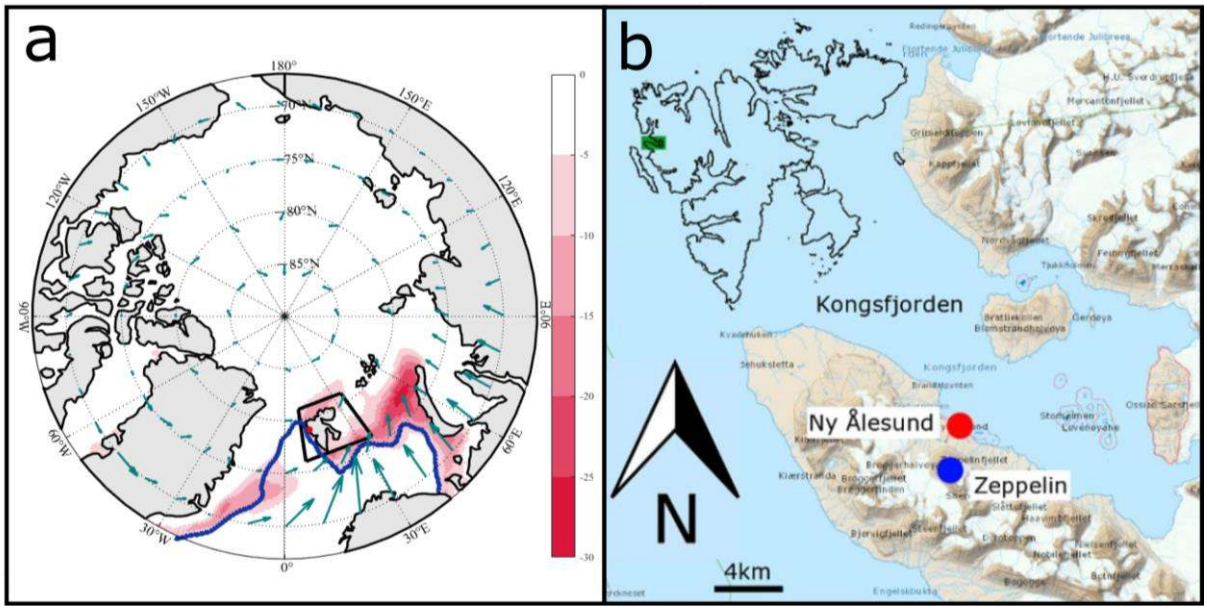

Figure 1. a) Linear trend (% per decade) of winter maximum sea-ice concentration from ERA-5 reanalyses (over the 1979-2018 period) in pink; mean-sea ice extent in March (blue line); integrated horizontal vapor fluxes (DJF) are plotted on some grid points (green arrow lengths

are proportional to vapor flux in kg.m^{-1}.s^{-1}). The area delineated by the black line corresponds to ERA 5 selected grid points used in supporting information Figure S1. b) Map of Kongsfjorden, Svalbard (*modified* from Eckhardt et al. (2013))*: Ny-Ålesund (8 m a.s.l.) and Zeppelin (474 m a.s.l.).*

Water stable isotopes are a classical tool to study the organization of the atmospheric water cycle (Gat, 1996; Jouzel, 2003). We use the δ notation to express the ratio (in per mil, ‰) between heavier ($HD^{16}O$ or $H_2{}^{18}O$) molecules and lighter molecules ($H_2{}^{16}O$): $\delta=(R_{sample}/R_{VSMOW}-1)*1000$ where R_{sample} is the ratio between heavier and lighter water molecules of measured sample and R_{VSMOW} is the ratio between heavier and lighter water molecules of the reference water (Vienna Standard Mean Ocean Water). In polar continental regions such as Greenland or the East Antarctic plateau, $\delta^{18}O$ and δD are closely controlled by changes in temperature along the trajectory from the warm regions of evaporation to the polar regions leading to a distillation process and thus a decrease in the heavy isotope content in atmospheric water vapor (Jouzel et al., 2013; Masson-Delmotte et al., 2008). In addition, the second-order parameter, d-excess (d-excess = $\delta D - 8* \delta^{18}O$, Dansgaard, 1964) brings complementary information on the climatic conditions of the source evaporative region and moisture recycling over the distillation path. Variations in d-excess result from different sensitivities of δD and $\delta^{18}O$ to kinetic fractionation processes such as diffusion during evaporation and moisture uptake occurring along the atmospheric transport pathway (Craig & Gordon, 1965). During evaporation over the ocean, high (low) relative humidity levels lead to small (high) kinetic fractionation hence low (high) d-excess. The combination of $\delta^{18}O$ and δD can thus provide quantitative insights on the origin and dynamics of moisture trajectories. Bonne et al. (2014) have shown that this initial d-excess signal is partially preserved during moisture transport towards Greenland. During snow formation, kinetic effects are also at play, especially for situation of high supersaturation, and they affect the d-excess values in polar regions (Jouzel & Merlivat, 1984).

Until recently, water isotopes measurements were only possible on the condensed phase, hence limiting their use to the study of atmospheric water cycle of rain and snowfall events . Some early studies performed water vapor analyses by trapping water vapor in a cold trap for several hours to get sufficient water for liquid analyses (Angert et al., 2004; Steen-Larsen et al., 2011). The recent progress of optical spectroscopy now permits the continuous measurement with high accuracy of the water vapor isotopic composition (Aemisegger et al., 2012; Galewsky et al., 2016; Tremoy et al., 2011). This new ability to monitor continuously δD and $\delta^{18}O$ of the water

vapor has been implemented during several measurement campaigns in different Arctic environments: over the Greenland ice sheet in summer (Berkelhammer et al., 2016; Steen-Larsen et al., 2013, 2014), in the marine boundary layer during oceanic campaigns on research vessels (Benetti et al., 2017; Bonne et al., 2019), as at coastal sites (Bonne et al., 2014; Kopec et al., 2014; Steen-Larsen et al., 2015), or in more continental and vegetated area like Siberia (Bastrikov et al., 2014). While being very useful to characterize the water cycle dynamics over a period in the region of interest, there are some limitations in the series already available. For example, none of the aforementioned records exceeds 12 consecutive months of monitoring at the same place, while at least 24 months would be needed to study interannual variations of the vapor isotopic composition.

With the aim to study the changes of origin of moisture trajectories to the Arctic region and the link with synoptic variability at seasonal and interannual scales, we installed a laser spectroscopy instrument to monitor the evolution of $\delta^{18}O$ and δD at Ny-Ålesund AWIPEV station, Svalbard (8 m a.s.l., Figure 1). It results in the longest time series record of water vapor stable isotopic composition (4.5 years), a period characterized by the highest mean annual temperature over the 1979-2018 period (-1.1°C in 2016) and by a low sea ice extent, as shown in Figure S1. This record has been completed with a comparison to measurements of water vapor isotopic composition at the neighbor site of Mount Zeppelin (474 m a.s.l.). Additionally, meteoric water samples were recovered at Ny-Ålesund AWIPEV station during each precipitation event, rainfall or snowfall.

This paper is organized into three sections. In section 2, we present the methods used to obtain, calibrate and validate the 4.5-year records of water isotopic composition in vapor and in precipitation, as well as meteorological data at the study site and methods to retrieve 5-day back trajectories. Section 3 presents the full dataset. Section 4 focuses on the information brought by water isotopes to document the origin of moisture arriving to Svalbard during winter humidity peaks.

2. Data and Methods

2.1. Meteorogical data

Meteorological data are available since 1993 at the AWIPEV observatory (Maturilli, 2020a). Hereafter, we use the 2-meter air temperature (°C), the specific humidity (volume mixing ratio in ppmv), the cloud base (CLB) height (m) (Maturilli & Ebell, 2018) and the radiosonde

144 measurements (Maturilli, 2018, 2020b) from Ny-Ålesund station provided by the Alfred
145 Wegener Institute – Research Unit Potsdam.
146
147 We also use outputs from the global atmospheric reanalysis of the European Center for
148 Medium-Range Weather Forecasts (ECMWF), ERA-5 6-hourly averaged data on pressure
149 levels from 1979 to 2018: the total daily precipitation amount (m), the sea ice area fraction, the
150 vertical integral of the water vapor flux ($\mathrm{kg.\,m^{-1}.\,s^{-1}}$) and the temperature (°C).
151
152 **2.2. Water vapor monitoring**
153
154 Two Picarro laser spectrometer instruments based on the cavity ring-down spectroscopy
155 (CRDS) technique were installed in Ny-Ålesund (8 m above sea level), in the AWIPEV
156 observatory building (Figure S3; Text S3): a L1102-i Picarro instrument from May 2014 to
157 May 2015 and then a L2130-i Picarro instrument until the end of the measurement campaign
158 (27/09/2018). The change of instrument is justified by the enhanced performances of the more
159 recent L2130-i Picarro (precision of 0.1 ‰ and 0.8 ‰ for $\delta^{18}O$ and δD respectively, 30 second
160 injection at 2500 ppmv, measurement rate of 1 Hz) compared to the L1102-i Picarro (precision
161 of 0.2 ‰ and 1 ‰ for $\delta^{18}O$ and δD respectively, 30 second injection at 10000 ppmv,
162 measurement rate of 0.1 Hz) (Picarro Inc., 2009, 2016). The outside air was continuously
163 pumped through a heated sampling line installed along the building, with an inlet located 10 m
164 above the ground level. The instrumental transition occurred in two phases: first, the L2130-i
165 instrument was installed at Zeppelin observatory (474 m a.s.l., 1.2 km from Ny-Ålesund) and
166 operated in parallel with the L1102-i instrument at Ny-Ålesund during two weeks (06/05/2015
167 to 23/05/2015, Figure S4). It was then set up at Ny-Ålesund (8 m a.s.l.) to replace the L1102-i
168 instrument. The full data series at Ny-Ålesund (Figure 2) presents some missing measurements:
169 1) every day, 2 hours were dedicated to standard measurements for calibration; 2) some longer
170 periods (e.g. from 23/04/2016 to 11/05/2016) were dedicated to the maintenance of the set-up.
171
172 The raw data from the CRDS instruments need to be calibrated as discussed previously in
173 several publications to ensure consistency with the international VSMOW-SLAP scale
174 (International Atomic Energy Agency, 2006). The volume water vapor mixing ratio in ppmv,
175 hereafter referred to as humidity, is continuously measured by the CRDS instrument. A
176 multiplying correction factor (0.91 and 1.02 respectively for our L1102-i and L2130-i

177 instruments) is applied to the measured humidity in order to match the local meteorological
178 data from AWIPEV (Figure S5, Text S4 and Text S5).
179
180 Following the protocol outlined in previous publications (Bonne et al., 2014; Steen-Larsen et
181 al., 2014; Tremoy et al., 2011), three main corrections are applied to the isotopic data to account
182 for: 1) the influence of humidity on $\delta^{18}O$ and δD measurement (Text S6), 2) the shift between
183 the measured values and the true isotopic values (Text S7), and 3) the temporal drift of the
184 instrument (Text S7), which refers to the temporal evolution of the shift between measured and
185 true values (Figure S6). The calibration set-up introduces vapor into the instrument with a
186 known isotopic composition at prescribed humidity levels (Text S4). The influence of humidity
187 on water vapor isotopic composition is determined during 2 calibration campaigns through a
188 series of measurements of water isotopic standard injected at different humidity levels (Figure
189 S7).

190 The isotope-humidity calibration determined for the second instrument is unfortunately more
191 scattered than for the first instrument below 2000 ppmv. It nevertheless shows that, above 2000
192 ppmv, the isotope vs humidity correction is small (< 0.1‰ and < 0.3 ‰ for $\delta^{18}O$ and δD,
193 respectively). The mean standard deviation is 1.3 ‰ (6.5 ‰) for $\delta^{18}O$ (δD) for measurements
194 performed at humidity levels lower than 2000 ppmv and 0.4‰ (1.4‰) for $\delta^{18}O$ (δD)
195 measurement performed at humidity levels higher than 2000 ppmv (Text S6 and Figures S6 and
196 S7). This study will thus focus on winter periods during which humidity values are higher than
197 2000 ppmv.
198
199 The other two corrections are calculated by measuring two water isotopic standards with
200 isotopic values bracketing the measured values at least once a day at constant humidity level
201 (set at 3700 ppmv between May 2014 and December 2016 and then at 6900 ppmv for the rest
202 of the campaign) (Texts S4, S7 and Figure S6). The uncertainty on the water vapor isotopic
203 data can then be calculated from the instrument replication (internal accuracy) and the
204 uncertainties associated with these corrections (Text S8, Figures S8, S9 and S10).
205
206 When the calibration system is working adequately (79% of the time), the uncertainty only due
207 to the reproducibility of daily standard measurements (including internal accuracy and
208 uncertainty on the drift of the instrument) is estimated to 0.11 ‰ for $\delta^{18}O$ and 0.70 ‰ for δD.
209 When no daily calibration is available (21% of the time), this uncertainty rises up to 0.18 ‰ for

$\delta^{18}O$ and 1.38 ‰ for δD. This uncertainty does not take into account possible biases due to variation of the influence of humidity on water vapor isotopic composition which is expected to be constant over the whole period of measurements according to our measurements (Text S6 and Figure S7) and previous study (Bailey et al., 2015).

2.3. Precipitation monitoring

Whenever precipitation events occurred, water or snow was sampled daily at midday and stored in a glass container at 8-10°C and shipped to LSCE for measurement. Altogether, 519 samples were collected over the 4.5 years. Samples were sent back to LSCE every 6 months. Water stable isotope measurements were performed with a Picarro CRDS instrument working in liquid mode, i.e. with vaporization of the samples in dry air to reach a humidity of 20,000 ppmv. Replicates were performed over 15% of the samples so that we could calculate the uncertainty (2σ) for our dataset to 0.05 ‰ and 0.2 ‰ respectively for $\delta^{18}O$ and δD.

2.4. Back-trajectories

The origin and trajectory of air masses were evaluated using the HYSPLIT model (Hybrid-Single Particle Lagrangian Integrated Trajectory) (Stein et al., 2015; http://ready.arl.noaa.gov/HYSPLIT_traj.php). In this model, the position of the air mass is determined using a three-dimensional Lagrangian air mass vertical velocity algorithm. The set of meteorological data used to simulate trajectories was taken from ERA-5. We have calculated 5 days back-trajectories with a single launch of one particle every 6 hours at 500 m.a.s.l. above Ny-Ålesund coordinates throughout the full data series period. Hysplit was used here to provide an estimate of the origin of air masses over specific moist events from our 4.5 years' dataset. We have chosen a 500 m.a.s.l altitude for the particle launch for several reasons. First, the vertical mixing in HYSPLIT is not ideally represented (Ngan et al., 2019) so that we expect artefacts when running the particle launch at 10 m.a.s.l. (where the inlet was actually located). Second, we checked that the temporal evolution of the water vapor isotopic composition is the same at 10 m.a.s.l. and 500 m.a.s.l. (section 3.4). Finally, a sensitivity test has been performed comparing back-trajectories at 500 m.a.s.l. and 10 m.a.s.l. on a 2-year period (June 2014 to September 2016) :only 20 back-trajectories over 308 have opposite origin when comparing those obtained from a launch of particles at 500 m.a.s.l. to those obtained from a launch of particles at 10 m.a.s.l. Despite being convenient to produce diagnostics over long-time series,

Hysplit has however some limitations. As Hysplit computations are based on single particle trajectories, the representativeness of our estimates might not be correct. To assess this point, we used in addition to Hysplit the Lagrangian Particle Dispersion Model Flexpart (Stohl et al., 2005) with a large ensemble of particles for a couple of selected events: every 6 hours a batch of 500 neutral inert air tracer particles are randomly released from a volume (0.1°x0.1°x100 m) centered around Ny-Ålesund coordinates (at an altitude of 50 m.a.s.l). Flexpart is driven by meteorological fields from ERA5 to compute 10-day back-trajectories. We developed visualization tools to display the concentration of particles being transported above each grid point in latitude-longitude and latitude-altitude maps (Text S9).

3. Results

In this section, we first present the full 4.5-year data set at Ny-Ålesund for the water vapor isotopic composition as well as its variability at the inter-annual, seasonal and diurnal scale. This data set is then compared to the short series of parallel measurements of the water vapor at the nearby site of Mount Zeppelin (474 m a.s.l.), and finally to the 4.5 years' record of meteoric water isotopic composition sampled at the event scale at Ny-Ålesund.

3.1 Isotopic composition of the vapor water at Ny-Ålesund and links with meteorological data

The full calibrated hourly data series spanning 4.5 years are displayed in Figure 2.

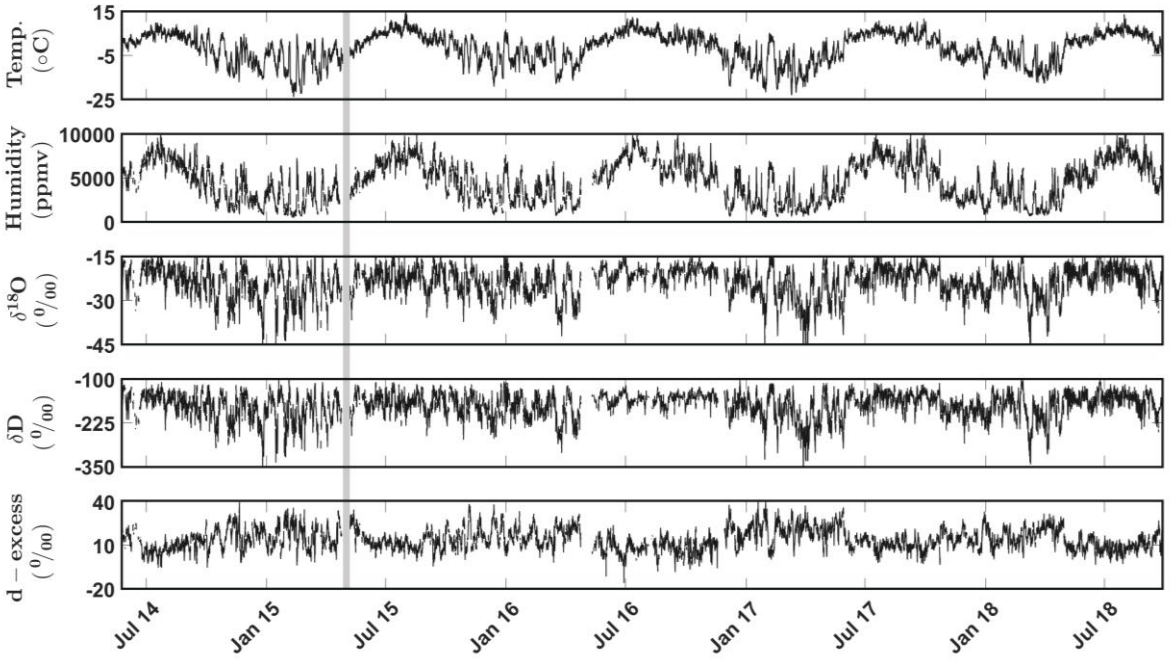

Figure 2. From top to bottom: temperature, humidity, $\delta^{18}O$, δD *and d-excess of atmospheric water vapor at 10 m. The full data series (black) was corrected following the calibration procedure described in Supporting Information Text S5, S6 and S7 and show clear seasonal variations. The grey period corresponds to the switch of instrument (from L1102-i to L2130-i). Note that different correction factors were implemented for the first instrument and the second one.*

Our dataset depicts a clear co-variance in temperature, humidity, and water vapor $\delta^{18}O$. On the contrary, we observe a global anti-correlation between d-excess and $\delta^{18}O$ (R=-0.68) or δD. The $\delta^{18}O$ vs temperature slope over the full record (Figure 3a) is 0.62 ‰.°C $^{-1}$ for the entire series

(0.78 ‰.°C $^{-1}$ when considering only winter, i.e. DJF). This relationship between water vapor $\delta^{18}O$ and temperature lies within previous estimates in the region. The temporal slope observed at the coastal Greenland site of Ivittuut is smaller (0.37 ‰.°C $^{-1}$, Bonne et al., 2014) and such a low value could be linked to the latitude of Ivittuut, lower than at Ny-Ålesund. Over the northwest Greenland ice sheet, the isotopic record of the NEEM station spans summer only, and is marked by strong diurnal cycles probably associated with local exchanges between snow surface and water vapor superimposed on the synoptic signal (Steen-Larsen et al., 2013). The NEEM dataset spanning 3 consecutive summer seasons is associated with a temporal slope of 1.1 ‰.°C $^{-1}$, i.e. almost twice larger than the $\delta^{18}O$ vs temperature slope of our record.

The observed relationship between humidity and water vapor $\delta^{18}O$ is displayed in Figure 3b. The general pattern is very close to the theoretical relationship between water vapor $\delta^{18}O$ and humidity predicted by a Rayleigh distillation along a trajectory starting from evaporation over the mid-latitude ocean (see black line in Figure 3b). The relatively low water vapor $\delta^{18}O$ values (-40 to -15 ‰) indicate that the recharge of water vapor by local ocean evaporation is small at least during winter. Indeed, the isotopic composition of water vapor evaporating over the open ocean in North Atlantic is about -8 to -20‰ (Benetti et al., 2017, 2018; Bonne et al., 2019; Steen-Larsen et al., 2015, 2017) so that a strong recharge would lead to higher $\delta^{18}O$ values than observed in winter. In summer, the relatively high values of $\delta^{18}O$ values of water vapor can be due to some local evaporation. The results obtained here suggest that the variability of the $\delta^{18}O$ signal in winter is driven by different degrees of distillation of advected air masses (Dansgaard, 1964; Rayleigh, 1902) in addition to a switch of distant moisture sources (Vázquez et al., 2016).

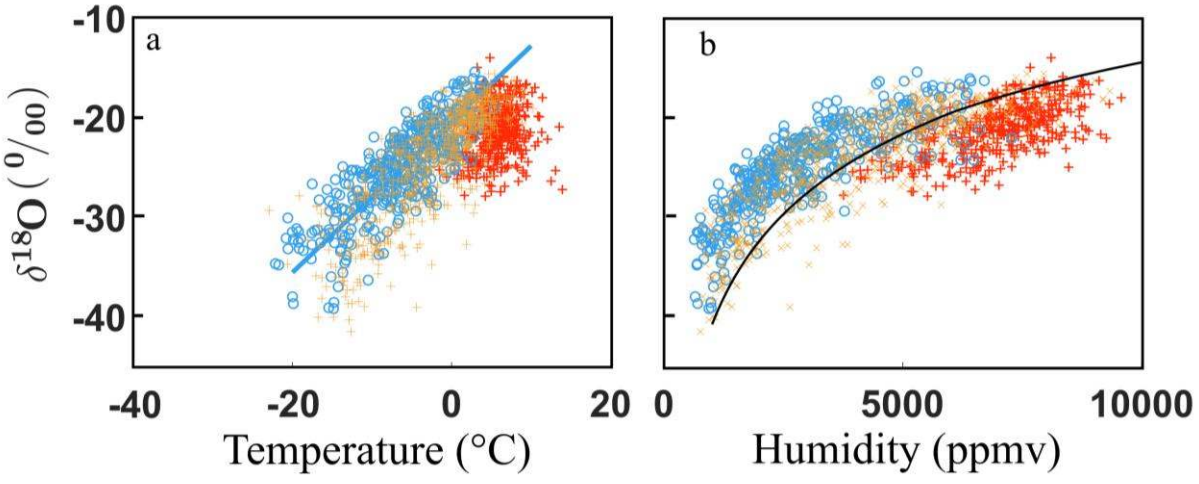

Figure 3. Observed relationship between surface water vapor $\delta^{18}O$ *and surface air temperature (a) and between surface water vapor* $\delta^{18}O$ *and humidity (b). The colors of data points vary*

according to the seasons: blue circles for winter (DJF), yellow crosses for autumn (SON) and spring (MAM), red crosses for summer (JJA) seasons. The blue line in Figure 3a is the linear fit between $\delta^{18}O$ *and temperature during winter (DJF), the black line in Figure 3b is the model output from MCIM (Mixed Cloud Isotopic Model,* Ciais & Jouzel, 1994*, initial conditions: surface pressure = 1015 hPa, surface temperature = 290K and surface relative humidity = 80%).*

3.2. Seasonal and diurnal variabilities

Seasonal variations are observed unequivocally in both temperature and humidity (Table 1) which reach maximum values in summer, respectively 5.0°C and 6900 ppm, and minimum values in winter, respectively -7.0°C and 2800 ppm (average values over JJA and DJF respectively over the whole time period). Similarly, higher values are observed in summer for water vapor isotopic composition (+4.1 ‰ and +25.5 ‰ in average for $\delta^{18}O$ and δD respectively compared to winter values), as expected from the temperature-to-isotopic composition relationship. The d-excess signal depicts lower values in summer than in winter, hence in anti-correlation with $\delta^{18}O$. This result is similar to observations by Bonne et al. (2014) in South Greenland but opposite to the d-excess maximum observed in summer precipitation in central Greenland (Kopec et al., 2019).

The intra-seasonal variability is much larger in winter than in summer: the winter standard deviation is almost twice larger for temperature, $\delta^{18}O$ and δD compared to summer. The humidity and d-excess variability is also larger in winter than in summer. The strong winter variability motivates us to explore the associated mechanisms and their potential links to synoptic scale events.

Year	Summer (JJA)						Winter (DJF)						Full year (Jan to Dec)					
	Hum (ppmv)	RH (%)	T (°C)	$\delta^{18}O$ (‰)	δD (‰)	d-xs (‰)	Hum (ppmv)	RH (%)	T (°C)	$\delta^{18}O$ (‰)	δD (‰)	d-xs (‰)	Hum (ppmv)	RH (%)	T (°C)	$\delta^{18}O$ (‰)	δD (‰)	d-xs (‰)
14	**6800** ±1200	**82** ±9	**3.9** ±2.3	**-20.9** ±3.2	**-158.7** ±21.9	**8.4** ±5.4	**2400** ±1400	**65** ±12	**-9.1** ±6.3	**-27.2** ±6.2	**-199.6** ±46.3	**17.6** ±7.3	//	//	//	//	//	//
15	**6900** ±1200	**76** ±11	**5.7** ±2.4	**-22.1** ±3.2	**-166.0** ±22.7	**10.6** ±3.6	**3000** ±1400	**69** ±11	**-5.7** ±4.9	**-25.0** ±4.3	**-183.9** ±32.2	**16.5** ±6.9	**4200** ±2200	**72** ±12	**-2.1** ±7.1	**-24.0** ±5.0	**-177.2** ±36.0	**14.9** ±7.5
16	**7000** ±1300	**77** ±11	**5.4** ±2.4	**-21.1** ±3.0	**-160.8** ±16	**8.3** ±5.4	**2700** ±1700	**67** ±14	**-8.2** ±6.2	**-25.0** ±4.9	**-180.7** ±35.4	**19.3** ±7.9	**4900** ±2200	**73.5** ±12	**-0.8** ±6.1	**-22.5** ±4.3	**-168.1** ±30	**12.2** ±7.4
17	**6900** ±1100	**79** ±9	**4.7** ±2	**-21.0** ±3.1	**-157.0** ±21.3	**11.0±** 4	**3100** ±1300	**66** ±12	**-4.9** ±4.1	**-24.0** ±4.0	**-177.8** ±30.9	**14.5** ±5.9	**4200** ±2400	**70** ±12	**-2.7** ±7.3	**-24.5** ±5.5	**-180.1** ±38.9	**15.9** ±7.5
18	**7000** ±1300	**78** ±9	**5.1** ±2.1	**-20.7** ±3.1	**-156.9** ±21.7	**8.9** ±4.4	//	//	//	//	//	//	//	//	//	//	//	//
TOT	**6900** ±1200	**79** ±10	**5.0** ±2.3	**-21.2** ±3.1	**-159.9** ±21.2	**9.5** ±4.7	**2800** ±1500	**68** ±12	**-7.0** ±5.7	**-25.3** ±5.1	**-185.4** ±37.6	**17.0** ±7.3	**4600** ±2300	**72** ±12	**-1.6** ±6.7	**-23.6** ±5.1	**-175.0** ±36.1	**14.0** ±7.4

Table 1. mean and standard deviation of meteorogical parameters and isotopic composition calculated from hourly means. Total standard deviation is calculated from the concatenated seasons at hourly resolution. Summer 14 corresponds to JJA of year 2014 and winter 14 corresponds to December 2014, January 2015 and February 2015.

In contrast with results of water vapor time series from sites marked by large diurnal variations in local boundary layer winds or evapotranspiration (Berkelhammer et al., 2016; Bréant et al., 2019; Kopec et al., 2014; Steen-Larsen et al., 2013), diurnal variations are very small in our record, with diurnal amplitudes of temperature, humidity or $\delta^{18}O$ variations below 2°C, 870 ppm and 3.2 ‰ respectively, independently of the season. In our dataset, the mean diurnal variations have values comparable to the lowest diurnal variability observed in polar sites marked by large boundary layer variations (Bréant et al., 2019). This implies that our record is moderately influenced by diurnal changes in local surface fluxes and boundary layer mixing. This supports the finding that the Svalbard surface water vapor isotopic composition does not bear a clear signature of exchange with the local oceanic surface on diurnal time scales.

3.3. Comparison between sea level AWIPEV and 474 m a.s.l. Zeppelin observatory isotopic vapor data

During 2 weeks, in May 2015, water vapor isotopic composition was measured at two sites in parallel (Figure S4). A very high correlation is observed between the two data sets ($R > 0.9$ for humidity and $\delta^{18}O$, $R = 0.8$ for d-excess), with only a slight offset for humidity (average mixing ratio of 4000 ppmv and 3900 ppmv for AWIPEV station and Mount Zeppelin respectively), and for the mean $\delta^{18}O$ (-24.0 ‰ and -23.3 ‰ for AWIPEV station and Mount Zeppelin respectively). Temperatures at both sites are well correlated ($R = 0.87$) during this period, but

show an average difference of -3°C between Mount Zeppelin and AWIPEV. The high correlation between the two temperature records agrees with the high co-variance between both isotopic signals but cannot explain why the offset between the two $\delta^{18}O$ series is smaller than expected from the temperature vs $\delta^{18}O$ slope determined in section 3.1. A better explanation for this small shift is probably to be found in calibration issues with the Mount Zeppelin instrument (Figure S7). In the following discussion, we mainly focus on the water isotopic variability, and our findings are not challenged by this offset.

The strong correlation between the vapor isotopic composition measurement datasets near the surface and at 474 m a.s.l. justifies the assumption that the variations of the water vapor isotopic signal at Ny-Ålesund reflect the dynamics of the lower troposphere moisture isotopic composition driven by large scale regional variability, and not local boundary layer dynamics or sources. This finding is also supported by the analysis of almost 20 years of radiosondes measurements in Svalbard (Maturilli & Kayser, 2017), showing that local boundary layer characteristics are directly influenced by large scale dynamics such as Arctic Oscillation changes, even in winter time when an inner fjord weather regime can superimpose.

3.4. Comparison between vapor and precipitation isotopic composition

The full data series of the isotopic composition of precipitation together with surface air temperature measurements during precipitation days is presented in supporting information (Text S10 and Figure S11). The average $\delta^{18}O$ and d-excess over the measurement period are -9.6 ± 4.6 ‰ and 6.2 ± 10.5 ‰ with significant seasonal variations. The variability is twice larger during winter than during summer for $\delta^{18}O$, as already observed for the vapor isotopic composition (Table 1). This is mainly due to the large range of temperature variations in winter compared to summer (factor of 2 between both variabilities).

The precipitation $\delta^{18}O$ values observed at Ny-Ålesund are coherent with the precipitation $\delta^{18}O$ values in the Arctic region as documented by the IAEA/WMO Global Network for Isotopes in Precipitation (GNIP) database with monthly $\delta^{18}O$ values varying between -9 and -17 ‰ in North Sweden. In Ivittuut (Greenland), Bonne et al. (2014) also found similar $\delta^{18}O$ values for precipitation between -5 and -20 ‰. Svalbard Ice core $\delta^{18}O$ variations from (Isaksson et al., 2005) show a range of more depleted $\delta^{18}O$ values (around -16 to -17‰), which are consistent with a stronger distillation towards higher altitudes (drilling altitude of ice cores of 1250 and 750 m, respectively) than for a coastal site such as Ny-Ålesund (Smith & Evans, 2007; Stern & Blisniuk, 2002).

In order to compare the precipitation isotopic signal to the vapor signal, we calculated the theoretical isotopic composition of a vapor at equilibrium with each precipitation sample. Equilibrium fractionation coefficients are temperature-dependent and it is not obvious to define which equilibrium temperature should be used within the atmospheric column between the cloud base (where precipitation forms) and surface temperature (where liquid precipitation can be reequilibrated with the surrounding water vapor measured by the Picarro instrument). Several sensitivity tests were performed (Text S10 and Figure S12) and equilibrium fractionation coefficients were finally computed with 2-meter air temperature for rain samples (because of possible exchange with water vapor at this sampling height), and with cloud base height temperature for solid precipitation. Indeed, we assumed that the isotopic composition of snow does not significantly change during its descent and possible partial sublimation along the atmospheric column (Maturilli & Kayser, 2017). For our calculation, we used liquid-vapor and solid-vapor fractionation coefficients at equilibrium from Majoube (1971) and Merlivat and Nief (1967).

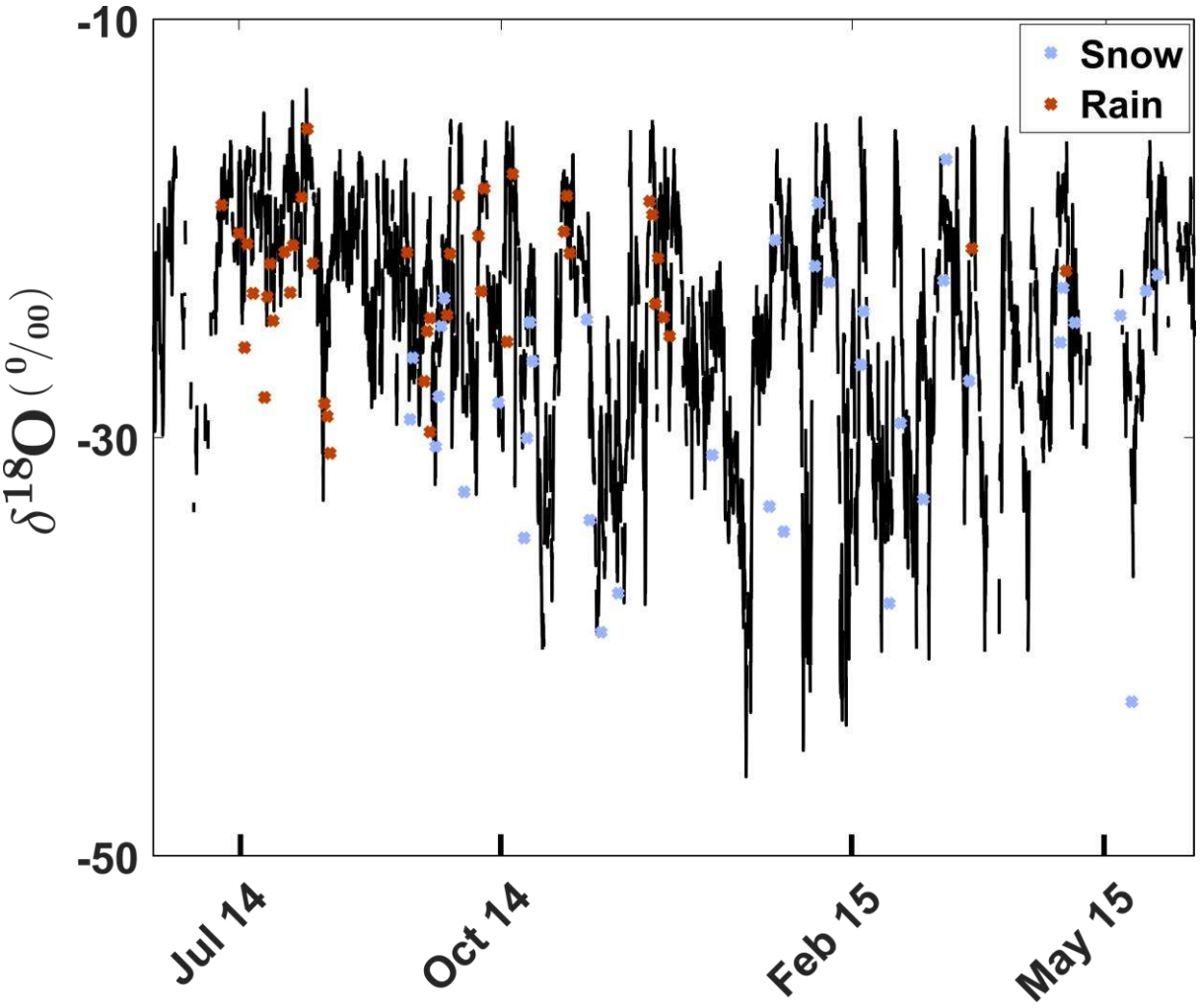

391 *Figure 4. Comparison over one-year (from 01/06/2014 to 01/06/2015) of the* $\delta^{18}O$ *measured in*
392 *the vapor (black line, hourly averaged) and the theoretical computed* $\delta^{18}O$ *of vapor in*
393 *equilibrium with precipitation samples collected daily at AWIPEV station (light blue for snow*
394 *and red for rain).*

395 Figure 4 and Figure S13 show the reconstructed water vapor $\delta^{18}O$ series calculated from
396 precipitations (see also Figure S12 and S13) along with the $\delta^{18}O$ directly measured in the vapor.
397 Both $\delta^{18}O$ series share around 60% of variance (R=0.78). Such a good correlation shows that
398 synoptic events affecting the water vapor isotopic composition should also be recorded in the
399 snow and rain when these synoptic events are associated with precipitation. The remaining
400 unexplained variance can be due to kinetic effects occurring 1) during precipitation re-
401 evaporation within the atmospheric column or most probably during the 24 hours' period
402 between precipitation and sampling, 2) during precipitation formation in supersaturation
403 condition or mixed-phase clouds.

404 **4. Investigation of winter synoptic events and perspectives**

405 From the absence of a significant diurnal cycle, the coherency between day-to-day variations
406 recorded in vapor and precipitation isotopic measurements, as well as the similarity between
407 data from stations at two different altitudes, we have demonstrated that the signal recorded at
408 AWIPEV is dominated by day-to-day variability associated with synoptic weather. We can
409 hence use surface vapor measurements to study large scale processes in this sector and we
410 concentrate in the following on the important winter variability of temperature, humidity and
411 water stable isotopes. Moreover, Rinke et al. (2017) and Zhang et al. (2004) have shown that
412 the cyclone intensity and frequency are higher in winter which makes this season of particular
413 interest for the Svalbard region.

414 **4.1. Detection of synoptic events**

415 We first characterize the signature of synoptic events on the vapor isotopic composition from
416 our time series. Synoptic events are defined as events of a time scale of 1 to 5 days and a spatial
417 scale of several hundred to several thousand kilometers. In the Arctic, increases of the humidity
418 of 3000 ppmv within a period of two days, following the criteria used by Bonne et al., (2014),
419 are associated with synoptic events, particularly in winter when almost all events are linked to
420 anomalies in temperature due to air masses coming from the North Atlantic (Nomokonova et
421 al., 2020). We use these criteria to identify the humidity peaks from our time series in Svalbard
422 and pinpoint synoptic events. During the period from 01/06/2014 to 01/06/2015 (Figure 5),

these large and abrupt events provide 39% of the total precipitation amount (as identified using ERA5 total precipitation variable) and are associated with large peaks in the water vapor isotopic composition, i.e. a systematic increase in $\delta^{18}O$ and in most cases a decrease in d-excess.

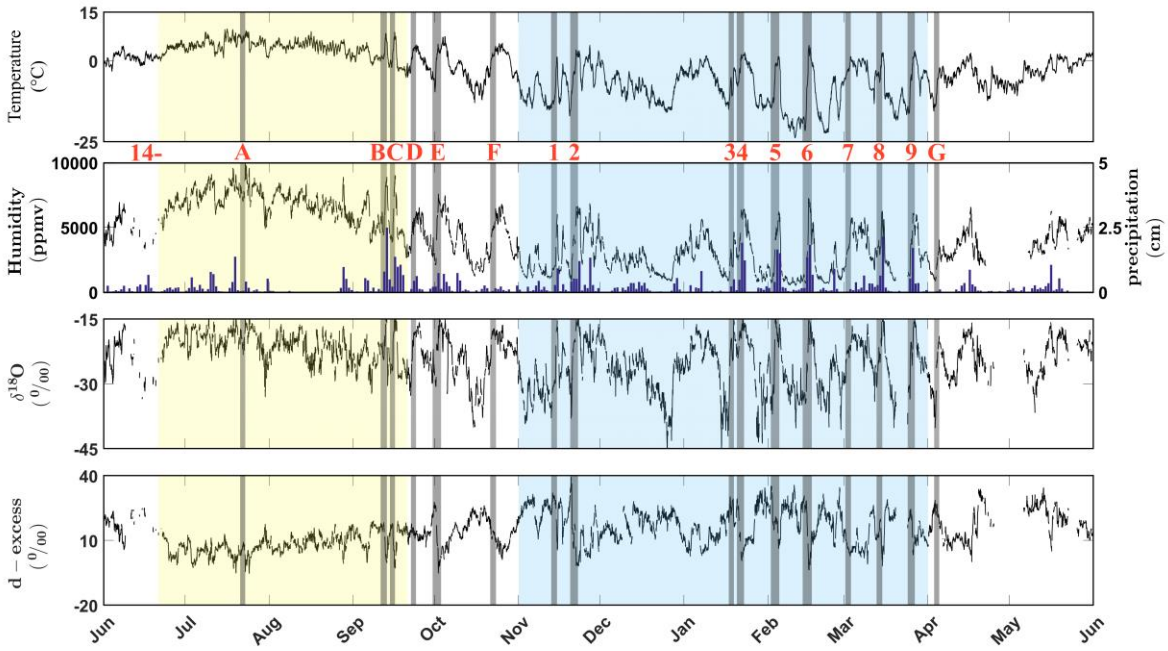

Figure 5. One-year data series (01/06/2014 to 01/06/2015) of measurements at AWIPEV station. Blue bars in the second panel stand for daily precipitation amount derived from ERA-5. In yellow: summer season, in blue: extended winter season (from November to March). Grey bars are humidity peaks defined as an increase of 3000 ppmv (or more) within 2 days (numbered from 14-1 to 14-9 during extended winter, and from 14-A to 14-G out of this period).

Over the full year period, we identify 16 such synoptic events numbered 14-1 to 14-9 and 14-A to 14-G: only 3 are detected during the warm plateau in summer (14-A, 14-B and 14-C in Figure 5), 2 of them occurring at the very end of the summer period when temperature and humidity start to decrease (14-B and 14-C). The other 13 occur outside of this period. Winter climate variability is dominated by the moist events occurring 5 to 9 times between the months of November and March, which is consistent with the relatively high increase of vertically integrated water vapor content in the region in winter (Nomokonova et al., 2020; Rinke et al., 2019). In the following, we thus focus this study on the humidity peaks over the coldest period (i.e. temperature below 5°C, large predominance of snow precipitation) from 1st November to 31st March, hence events 14-1 to 14-9 in Figure 5 and Figure 6. Moreover, such events are expected to be an important signal in the accumulated snow in the region which has a direct application for the interpretation of ice cores (Divine et al., 2008; Isaksson et al., 2005; Opel et

al., 2009). These nine events, each one associated with a temperature increase larger than 7°C, systematically display an increase in $\delta^{18}O$ larger than 7 ‰ within 2 days. The d-excess generally shows a decreasing signal larger than 10 ‰ within 2 days (observed for all events except for 14-3).

The same detection routine (increase of more than 3000 ppmv in 2 days) is then applied over the four winters (November to March) of our record, for years 2014 to 2018. In total, we detect 28 events (Figure 6 for winter 14, Figure S14 for following years). All of these humidity events display a significant increase of $\delta^{18}O$ (more than 7 ‰ in 2 days). A majority of these peaks seem associated with a decrease of d-excess.

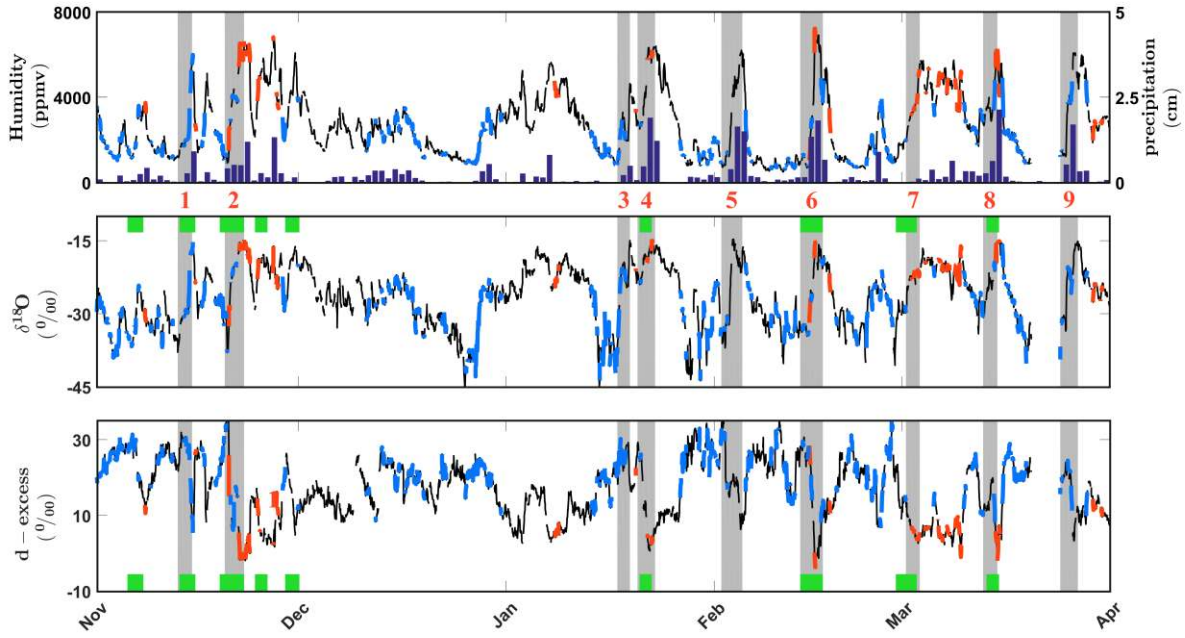

Figure 6. Links between the water vapor isotopic composition and air mass origin over winter 14. Grey bars are humidity peaks as defined in the text. Red and blue lines correspond to air masses with specific source location (North Atlantic and Arctic respectively) estimated with Hysplit (see text). Time periods with particularly high anti-correlation (R<-0.7) between $\delta^{18}O$ and d-excess are highlighted by the green bars.

4.2. Possible mechanisms at play

As mentioned in the introduction, d-excess variations can be used to trace changes in moisture sources. We investigate here how the combination of surface vapor $\delta^{18}O$ and d-excess can provide information on the origin of the air mass trajectories coming to Svalbard during our winter humidity peaks. For this purpose, we calculate the correlation coefficient between the

increase of $\delta^{18}O$ and the corresponding hourly variation of d-excess over the 2 consecutive days of one identified humidity peak. We tag in green in Figure 6 and Figure S14 the time periods with both (i) a significant increase in $\delta^{18}O$ (>7 ‰) and (ii) a significant anti-correlation between d-excess and $\delta^{18}O$ (R<-0.7).

Several explanations can be proposed for the observed anti-correlation between d-excess and $\delta^{18}O$ over the highlighted green periods. A first effect can be linked to the role of precipitation and transport. A $\delta^{18}O$ vs d-excess anti-correlation can be obtained in the case of intense distillation as observed in the water vapor isotopic composition in continental polar regions after a long trajectory without significant recycling or high in the atmosphere (Risi et al., 2010; Touzeau et al., 2016). This effect could play a role in the polar Svalbard context and can best be evidenced using a logarithm definition of the d-excess (Dütsch et al., 2017; Uemura et al., 2012), see details in Text S2 and Figure S2. Still, the observed range of $\delta^{18}O$ values is rather high, ruling out a case of intense distillation. The other dominant effects are linked to evaporation and re-evaporation which occur along the water mass trajectory. Because of kinetic effects, evaporation of water under relatively dry air conditions should lead to lower $\delta^{18}O$ and higher d-excess in vapor, based on the simple approach of Merlivat and Jouzel (1979) applied to several systems (e.g. Sodemann et al., 2017); this effect probably plays a role here. Then, as shown in Risi et al. (2008), re-evaporation is one of the major processes explaining the isotopic signal in regions with strong local precipitation, characterized by the so-called amount effect (decrease in $\delta^{18}O$ and increase in d-excess for strong precipitation rate). Rain re-evaporation leads to an increase of d-excess in the water vapor. However, this effect is dominant mostly in tropical regions or below clouds in case of dry air advection from the free troposphere. We are studying here moist events with a large proportion of snow precipitation so that rain re-evaporation is probably not the main driver of our isotopic signal. Finally, another possible process is the sublimation of snow (Kopec et al., 2019; Pang et al., 2018). However, sublimation of snow is an effect that is only significant in the continental polar regions when moisture travels above the continental ice sheet, which differs from our coastal Svalbard context.

We thus conclude that the process explaining the largest part of the d-excess vs $\delta^{18}O$ relationship in the water vapor over Svalbard is most likely linked with a change in evaporative conditions in the moisture source region. In particular, low d-excess is generally associated with high relative humidity at evaporation because kinetic fractionation is reduced when the air is saturated with water vapor. Where relative humidity of the atmosphere is low, for instance near the sea ice margins or during SLOE events (Strong Large-scale Ocean Evaporation), d-excess

values in surface vapor are high (Kurita, 2003). This mechanism has already been proposed to explain high d-excess values observed in the Arctic region (Aemisegger, 2018; Aemisegger & Sjolte, 2018; Bonne et al., 2019; Steen-Larsen et al., 2015) and should also be considered to understand our records. Because of the probable influence of source evaporative conditions and distillation along the trajectory on the isotopic signal, we thus focus in the following on the role of changes in air mass trajectories and origin of air massesusing back-trajectories calculated for each wet winter (humidity peak) event.

4.3. Back-trajectories and isotopic signature

The Hysplit back-trajectories were first clustered according to their origin: the back-trajectories with their origin (first 2 days) within the Arctic sector (latitude higher than 80°N and longitude between 60°W and 60°E) are displayed in blue; the back-trajectories with their origin within the Atlantic sector (latitudes below Iceland are displayed in red (Figures 6, 7 and S14).

Year	14									15							16							17					Tot
Humidity peaks number	1	2	3	4	5	6	7	8	9	1	2	3	4	5	6	7	1	2	3	4	5	6	7	1	2	3	4	5	28
Atlantic source		X		X		X	X	X		X		X	X		X	X		X			X	X	X		X	X	X	X	18
Other source	X		X		X				X		X			X			X		X	X				X					10
(δ^{18}O,d-excess): R<-0.7	X	X		X		X	X	X		X	X	X	X			X					X		X			X			14
(δ^{18}O,d-excess): R>-0.7			X		X				X					X	X		X	X	X	X		X		X	X		X	X	14

Table 2. Classification of extended winter humidity peaks (Figure 6 and Figure S14). "Atlantic source" means that humidity peaks are associated with North Atlantic air masses while "other source" mainly stands for Arctic origins. The last two lines separate events associated with a specific isotopic signature (high anti-correlation between $\delta^{18}O$ and d-excess: R<-0.7) from others (no high anti-correlation between $\delta^{18}O$ and d-excess or positive correlation). Red boxes: moist events associated with North Atlantic origins based on the Hysplit diagnostic. Blue boxes: moist events mainly associated with Arctic origins based on the Hysplit diagnostic. The specific isotopic signature (fifth line) is most of the times associated with North Atlantic origins (red boxes). On the fifth line (sixth line), blue boxes (red boxes) contradict the general interpretation. Grey boxes: events for which back-trajectories are shown in Figure 7.

When comparing the anti-correlation between $\delta^{18}O$ and d-excess with the air mass origin over Svalbard, we observe that in most of the cases, the synoptic events with strong $\delta^{18}O$ vs d-excess

anti-correlation (14 events) are associated with an air mass origin located in the north Atlantic during the humidity peak (Table 2, 12 peaks over 14). For all these 14 events, air masses have an Arctic origin prior to the humidity increase. On the other hand, out of the 14 events with no clear anti-correlation detected, 8 are related to different air mass source (Table 2) mainly from the Arctic sector (Greenland, Siberia or Scandinavia). However, for 6 events (bold in the last column of Table 2), there is no clear anti-correlation between $\delta^{18}O$ and d-excess although air originates from the North Atlantic. We now illustrate in Figure 7 these different behaviors by focusing on 4 particular humidity peaks (16-5, 15-2, 17-1, 16-2) and complementing then by the Flexpart diagnostic (Text S9, Figures S15)

The humidity peak 16-5 (Figure 7, first panel) has a water isotopic signal showing a clear anti-correlation between the abrupt increase in $\delta^{18}O$ (more than 9 ‰) and the abrupt decrease in d-excess (more than 10 ‰) over 2 consecutive days (1-3 February). In parallel, back-trajectories shift rapidly (in less than one day) from a situation with air of Arctic origin to a situation with air of Atlantic origin. This example illustrates the general behavior observed for events marked in red on the fifth line in Table 2: an anti-correlation between the increase of $\delta^{18}O$ and the decrease of d-excess over winter humidity peak is the signature of a rapid shift of air origin from Arctic origin to oceanic mid-latitude (Atlantic region). Flexpart footprints help us to refine the location of the air parcel origin and allow us to relate this characteristic isotopic signature to a shift to a source located in the North Atlantic Ocean at a latitude below 60°N (Figure S15).

For only two events out of the 14 events identified over the winters of our study (14-1 and 15-2), the anti-correlation between an increase in $\delta^{18}O$ and a decrease in d-excess is not associated with a shift of moisture origin toward the Atlantic Ocean (Table 2). During the event 15-2 (second panel of Figure 7), air origin shifts from the Arctic ocean covered by sea ice to open waters of Barents and Greenland seas. We propose that this strong change of air mass origin can lead to the observed isotopic signal. This shift in air mass origin is confirmed by additional footprints analyses performed using the Flexpart tool: a large fraction of Flexpart back-trajectories show an origin of air mass in the atmospheric boundary layer above Arctic sea-ice before the humidity peak to a local source, suggesting that the moisture increase results from local evaporation (Figure S15).

14 events do not show any strong anti-correlation between $\delta^{18}O$ and d-excess (Table 2, last column). In a majority of cases (8 peaks over 14), the shift of air mass trajectories happens within the Northern sector (Arctic: Greenland, Siberia or Scandinavia). This is the case of the humidity peak beginning on 16 December 2017 (event 17-1, third panel of Figure 7): the $\delta^{18}O$

558 increase (more than 12 ‰) and the following decrease (slightly less than to 8 ‰), are not anti-
559 correlated with the d-excess signal. In fact, the d-excess is correlated with $\delta^{18}O$ ($R > 0.7$) during
560 the abrupt increase in humidity. In parallel, the back-trajectories display a change in the origin
561 of air parcels within the Northern sector: from continental region of Siberia (14-18 December)
562 to sea ice margin close to Svalbard (18-20 December). At the beginning of the event, relatively
563 low d-excess could be explained by soil evaporation in the Siberian continental regions
564 (Aemisegger et al., 2014). At the humidity maximum, the d-excess decrease can be explained
565 by local oceanic evaporation in a moist atmosphere, hence under a small air-sea humidity
566 gradient. The pattern of change in air mass origin is confirmed by the Flexpart footprints
567 analysis (Figure S15, third panel).

568 For the other events (15-6, 16-2, 16-6, 17-2, 17-4 and 17-5) during which the change of air mass
569 origin (from Arctic to North Atlantic origin) is not associated with d-excess vs $\delta^{18}O$
570 anticorrelation signature, the shift of air mass origin is either too slow or does not involve
571 latitudes southern than 65°N to be imprinted in the water isotopes records as illustrated for event
572 16-2 in Figure 7 (fourth panel). This conclusion is strengthened by Flexpart footprints which
573 show that the red back-trajectories computed with Hysplit can be misleading: at the humidity
574 maximum, most of the air masses originate in fact locally, from areas located at amplitudes
575 higher than 70°N of the Greenland Sea (Figure S15, fourth panel). This explains why the
576 isotopic signal is ambiguous over this particular event.

577

578

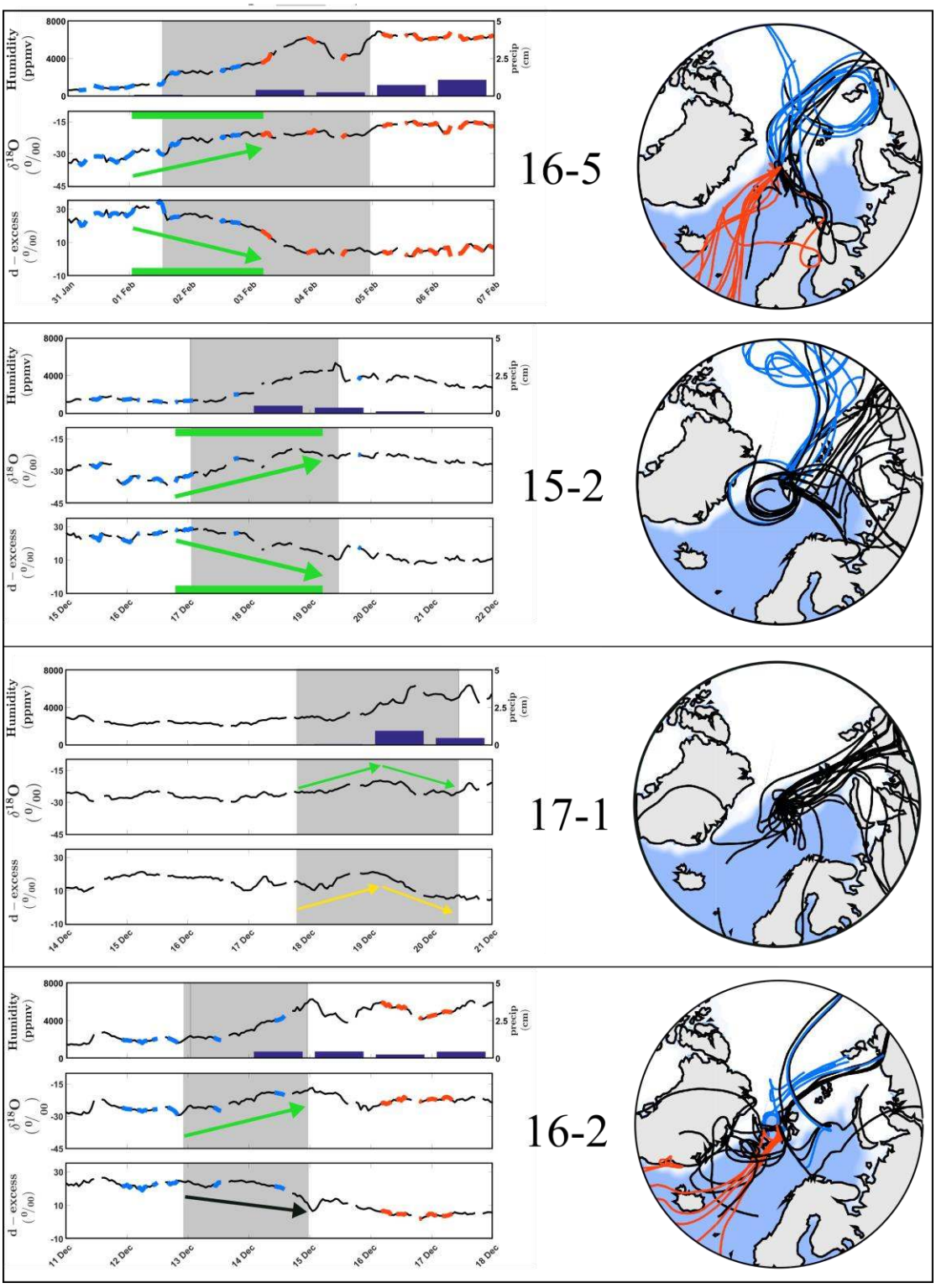

Figure 7. Examples of 4 humidity peaks (16-5, 15-2, 17-1, 16-2). The left panels display the humidity, precipitation, $\delta^{18}O$ and d-excess records over 7 days including the humidity peak event (in grey). The right panels display the associated 5 days back-trajectories computed with Hysplit. On both panels, red lines are for air parcel originating from the North Atlantic sector (first 2 days over the 5 days of calculation), while blue lines stand for the Arctic sector. Black

585 *lines and black back-trajectories are unlabeled. Arrows indicate the correlation between $\delta^{18}O$*
586 *and d-excess: pairs of green arrows are for high anti-correlation, pairs of green and yellow*
587 *arrows are for high correlation and a pair of green and black arrow stands for no specific*
588 *correlation. Sea ice concentration is represented in white (calculated from ERA-5 reanalyses).*
589

590 **4.4. Implications**

591 Our exceptionally long water vapor isotopic dataset complements previous findings from
592 records of isotopic composition of water vapor in the North Atlantic and Arctic regions. In
593 particular, Bonne et al. (2015) also identified synoptic events during autumn, winter and spring
594 associated with the same kind of humidity peaks (more than 3000 ppmv increase in 2 days) in
595 Greenland at the Ivittuut station. In their study, all identified humidity peaks display a strong
596 anti-correlation between a $\delta^{18}O$ increase and a d-excess decrease and all events correspond to
597 an arrival of moisture from the Atlantic Ocean, south of Greenland. Such a pattern agrees with
598 our finding over the Svalbard region, i.e. the anti-correlation between $\delta^{18}O$ and d-excess
599 indicates a shift to Atlantic origin for the air masses during the cold season humidity peaks.
600 However, such an isotopic signature for an Atlantic moisture origin has more implications in
601 Svalbard since a significant proportion of air masses during humidity peaks does not come from
602 the Atlantic, opposite to South Greenland where humidity peaks systematically originate from
603 the Atlantic. Water isotopes bring thus a strong added value to identify shifts in Svalbard air
604 mass origins.

605 Our results have implication for the interpretation of d-excess in the Arctic region. While, high
606 d-excess values observed in the Arctic regions have been associated with moisture source in
607 high latitude regions covered by sea-ice (Kurita, 2003, Bonne et al., 2019; Steen-Larsen et al.,
608 2015), others suggest that a switch in moisture sources from low to high latitude should result
609 in a decrease of d-excess (Kopec et al., 2019). Our study rather confirms the pattern where air
610 masses coming from high latitude carry vapor with higher d-excess: in fact, the humidity peaks
611 associated with air originating from the Arctic do not show any d-excess decrease, but rather
612 an increase as observed during events 14-9, 16-3, 17-1, 17-2, 17-5 with relatively high d-excess
613 values and positive correlation between $\delta^{18}O$ and d-excess.

614 First, the moist winter events are a significant source of precipitation over Svalbard. Our results
615 also have implications to be further explored in ice core science and climate modelling. From
616 the links made between vapor and precipitation measurements (section 3.4.), their isotopic

fingerprints archived in snow could help deciphering past changes in the origin of moisture coming to the Arctic region using Svalbard ice core records.

Second, Svalbard is a key location to look at the atmospheric circulation and transport of moist air at the boundary between north Atlantic and Arctic with a possible large influence of the sea ice. Isotopic composition of water vapor brings an important diagnostic on shift of air mass origin that should be combined with modelling approaches including water isotopes description. One of the largest limitations when dealing with isotope-enabled models is their inability to reproduce the large variations of d-excess in the north Atlantic and Arctic regions (Risi et al., 2010; Steen-Larsen et al., 2017; Werner et al., 2011). Part of this limitation may be linked to an inaccurate simulation of the water vapor isotopic composition in the boundary layer or during sublimation over the sea ice or over snow (Bonne et al., 2019; Kopec et al., 2019; Steen-Larsen et al., 2017; Werner et al., 2011). It may also be linked to an inaccurate transportation model of the atmospheric moisture (e.g. isotopic composition of water vapor is very sensitive to the model horizontal advection (Hendricks et al., 2000). Because Svalbard is at a key location with alternation of moisture arrival from Arctic and Atlantic, the comparison between our long water vapor isotopic record and atmospheric simulations may help disentangling the influence of marine boundary layer processes and atmospheric circulation.

Finally, our study focused on the large humidity peaks occurring during winter but there is a clear interest to look as well at the other circulation patterns during winter as well as other seasons with a possible larger influence of Arctic air masses. While the isotopic pattern is not as systematic as for the winter humidity peaks with North Atlantic origin, periods with moisture originating from the Arctic may be characterized by an opposite isotopic signature. However, Arctic air is often dry and calibration of water vapor isotopic record is still difficult at low humidity (below 2000 ppmv) hence limiting such an application (Casado et al., 2016; Ritter et al., 2016). A new generation of laser spectroscopy instrument and associated calibration set-up should soon permit to address such limitations. Our full dataset is available (Zenodo repository) and we encourage and welcome its use for other studies focusing on arctic air intrusions as well as on more local processes, such as polar lows or local orographic effects of air flows in the fjord.

5. Conclusion

We presented the first continuous multi-year record of water isotopes in surface water vapor at Ny-Ålesund (Svalbard), a key location at the edge of the current Arctic sea ice winter extent.

We have evidenced that this dataset reflects the regional dynamics of the atmospheric water cycle. In this region, winter weather regime is characterized by the recurrence of humid events lasting a few days. Combining $\delta^{18}O$ and d-excess in the water vapor with back-trajectories, we identify the isotopic signature of a shift of air mass origin from the Arctic to the North Atlantic below 60°N through a positive peak of $\delta^{18}O$ anti-correlated with d-excess. The isotopic signature of moisture transported from an Arctic source is less unequivocal but is generally marked by positive peaks of both $\delta^{18}O$ and d-excess.

Here, we focused our analyses on winter wet events, but our record can also be used to further explore the relationships between surface water vapor and precipitation isotopic composition and changes in air mass origins or moisture evaporation conditions during other seasons and at the inter-annual scale. This could be achieved using not only air mass back-trajectories as used here but also more sophisticated diagnoses of moisture transport and evaporation conditions (Papritz & Sodemann, 2018; Sodemann et al., 2008).

Acknowledgement:

This work was supported by the IPEV ARCTISO project, the ANR projects AC-AHC^2, GREENLAND, EAIIST and the LEFE program ADELISE. It was also funded by the Fondation Prince Albert 2 de Monaco under the project Antarctic-Snow. We thank Nick Hughes, from the Norwegian Meteorological Institute, for sharing sea ice observations, as well as Ove Hermansen from the Norwegian Institute for Air Research on behalf of the Norwegian Environment Agency. We acknowledge the staff from AWIPEV who took care of the experiment for almost 5 years and collected precipitation every day. We also thank two anonymous reviewers for their very useful comments regarding this paper.

Data Availability:

The full dataset archiving is underway and will be fully available through a Zenodo repository: 10.5281/zenodo.3689566. Until publication, the data set is with limited access.

References:

Aemisegger, F. (2018). On the link between the North Atlantic storm track and precipitation deuterium excess in Reykjavik. *Atmospheric Science Letters*, *19*(12), e865. https://doi.org/10.1002/asl.865

682 Aemisegger, F., & Sjolte, J. (2018). A Climatology of Strong Large-Scale Ocean Evaporation Events.
683 Part II: Relevance for the Deuterium Excess Signature of the Evaporation Flux. *Journal of*
684 *Climate*, *31*(18), 7313–7336. https://doi.org/10.1175/JCLI-D-17-0592.1
685 Aemisegger, F. (2018). On the link between the North Atlantic storm track and precipitation
686 deuterium excess in Reykjavik. *Atmospheric Science Letters*, *19*(12), e865.
687 https://doi.org/10.1002/asl.865
688 Aemisegger, F., & Sjolte, J. (2018). A Climatology of Strong Large-Scale Ocean Evaporation Events.
689 Part II: Relevance for the Deuterium Excess Signature of the Evaporation Flux. *Journal of*
690 *Climate*, *31*(18), 7313–7336. https://doi.org/10.1175/JCLI-D-17-0592.1
691 Aemisegger, F., Sturm, P., Graf, P., Sodemann, H., Pfahl, S., Knohl, A., & Wernli, H. (2012). Measuring
692 variations of δ ^{18} O and δ ^{2} H in atmospheric water vapour using two commercial
693 laser-based spectrometers: an instrument characterisation study. *Atmospheric Measurement*
694 *Techniques*, *5*(7), 1491–1511. https://doi.org/10.5194/amt-5-1491-2012
695 Aemisegger, F., Pfahl, S., Sodemann, H., Lehner, I., Seneviratne, S. I., & Wernli, H. (2014). Deuterium
696 excess as a proxy for continental moisture recycling and plant transpiration. *Atmospheric*
697 *Chemistry and Physics*, *14*(8), 4029–4054. https://doi.org/10.5194/acp-14-4029-2014
698 Alekseev, G., Kuzmina, S., Bobylev, L., Urazgildeeva, A., & Gnatiuk, N. (2019). Impact of atmospheric
699 heat and moisture transport on the Arctic warming. *International Journal of Climatology*,
700 *39*(8), 3582–3592. https://doi.org/10.1002/joc.6040
701 Angert, A., Cappa, C. D., & DePaolo, D. J. (2004). Kinetic 17O effects in the hydrologic cycle: Indirect
702 evidence and implications. *Geochimica et Cosmochimica Acta*, *68*(17), 3487–3495.
703 https://doi.org/10.1016/j.gca.2004.02.010
704 Arctic Monitoring and Assessment Programme. (2017). *Snow, Water, Ice and Permafrost in the Arctic*
705 *(SWIPA)*. Oslo, Norway:
706 Bailey, A., Noone, D., Berkelhammer, M., Steen-Larsen, H. C., & Sato, P. (2015). The stability and
707 calibration of water vapor isotope ratio measurements during long-term deployments.

Atmospheric Measurement Techniques, *8*(10), 4521–4538. https://doi.org/10.5194/amt-8-4521-2015

Bastrikov, V., Steen-Larsen, H. C., Masson-Delmotte, V., Gribanov, K., Cattani, O., Jouzel, J., & Zakharov, V. (2014). Continuous measurements of atmospheric water vapour isotopes in western Siberia (Kourovka). *Atmospheric Measurement Techniques*, *7*(6), 1763–1776. https://doi.org/10.5194/amt-7-1763-2014

Benetti, M., Steen-Larsen, H. C., Reverdin, G., Sveinbjörnsdóttir, Á. E., Aloisi, G., Berkelhammer, M. B., et al. (2017). Stable isotopes in the atmospheric marine boundary layer water vapour over the Atlantic Ocean, 2012–2015. *Scientific Data*, *4*(1), 160128. https://doi.org/10.1038/sdata.2016.128

Benetti, M., Lacour, J. -L., Sveinbjörnsdóttir, A. E., Aloisi, G., Reverdin, G., Risi, C., et al. (2018). A Framework to Study Mixing Processes in the Marine Boundary Layer Using Water Vapor Isotope Measurements. *Geophysical Research Letters*, *45*(5), 2524–2532. https://doi.org/10.1002/2018GL077167

Berkelhammer, M., Noone, D. C., Steen-Larsen, H. C., Bailey, A., Cox, C. J., O'Neill, M. S., et al. (2016). Surface-atmosphere decoupling limits accumulation at Summit, Greenland. *Science Advances*, *2*(4), e1501704. https://doi.org/10.1126/sciadv.1501704

Bintanja, R., & Selten, F. M. (2014). Future increases in Arctic precipitation linked to local evaporation and sea-ice retreat. *Nature*, *509*(7501), 479–482. https://doi.org/10.1038/nature13259

Bonne, J.-L., Masson-Delmotte, V., Cattani, O., Delmotte, M., Risi, C., Sodemann, H., & Steen-Larsen, H. C. (2014). The isotopic composition of water vapour and precipitation in Ivittuut, southern Greenland. *Atmospheric Chemistry and Physics*, *14*(9), 4419–4439. https://doi.org/10.5194/acp-14-4419-2014

Bonne, J.-L., Steen-Larsen, H. C., Risi, C., Werner, M., Sodemann, H., Lacour, J.-L., et al. (2015). The summer 2012 Greenland heat wave: In situ and remote sensing observations of water vapor

isotopic composition during an atmospheric river event. *Journal of Geophysical Research: Atmospheres*, *120*(7), 2970–2989. https://doi.org/10.1002/2014JD022602

Bonne, J.-L., Behrens, M., Meyer, H., Kipfstuhl, S., Rabe, B., Schönicke, L., et al. (2019). Resolving the controls of water vapour isotopes in the Atlantic sector. *Nature Communications*, *10*(1), 1632. https://doi.org/10.1038/s41467-019-09242-6

Bréant, C., Leroy-Dos Santos, C., Agosta, C., Casado, M., Fourré, E., Goursaud, S., et al. (2019). Coastal water vapor isotopic composition driven by katabatic wind variability in summer at Dumont d'Urville, coastal East Antarctica. *Earth and Planetary Science Letters*, *514*, 37–47. https://doi.org/10.1016/j.epsl.2019.03.004

Casado, M., Landais, A., Masson-Delmotte, V., Genthon, C., Kerstel, E., Kassi, S., et al. (2016). Continuous measurements of isotopic composition of water vapour on the EastAntarctic Plateau. *Atmospheric Chemistry and Physics*, *16*(13), 8521–8538. https://doi.org/10.5194/acp-16-8521-2016

Ciais, P., & Jouzel, J. (1994). Deuterium and oxygen 18 in precipitation: Isotopic model, including mixed cloud processes. *Journal of Geophysical Research*, *99*(D8), 16793. https://doi.org/10.1029/94JD00412

Craig, H., & Gordon, L. I. (1965). Deuterium and oxygen 18 variations in the ocean and the marine atmosphere.

Dahlke, S., & Maturilli, M. (2017). Contribution of Atmospheric Advection to the Amplified Winter Warming in the Arctic North Atlantic Region. *Advances in Meteorology*, *2017*, 1–8. https://doi.org/10.1155/2017/4928620

Dahlke, S., Hughes, N. E., Wagner, P. M., Gerland, S., Wawrzyniak, T., Ivanov, B., & Maturilli, M. (2020). The observed recent surface air temperature development across Svalbard and concurring footprints in local sea ice cover. *International Journal of Climatology*, joc.6517. https://doi.org/10.1002/joc.6517

758 Dansgaard, W. (1964). Stable isotopes in precipitation. *Tellus*, *16*(4), 436–468.
759 https://doi.org/10.1111/j.2153-3490.1964.tb00181.x
760 Ding, Q., Schweiger, A., L'Heureux, M., Battisti, D. S., Po-Chedley, S., Johnson, N. C., et al. (2017).
761 Influence of high-latitude atmospheric circulation changes on summertime Arctic sea ice.
762 *Nature Climate Change*, *7*(4), 289–295. https://doi.org/10.1038/nclimate3241
763 Divine, D. V., Isaksson, E., Pohjola, V., Meijer, H., van de Wal, R. S. W., Martma, T., et al. (2008).
764 Deuterium excess record from a small Arctic ice cap. *Journal of Geophysical Research*,
765 *113*(D19), D19104. https://doi.org/10.1029/2008JD010076
766 Dufour, A., Zolina, O., & Gulev, S. K. (2016). Atmospheric Moisture Transport to the Arctic:
767 Assessment of Reanalyses and Analysis of Transport Components. *Journal of Climate*, *29*(14),
768 5061–5081. https://doi.org/10.1175/JCLI-D-15-0559.1
769 Dütsch, M., Pfahl, S., & Sodemann, H. (2017). The impact of nonequilibrium and equilibrium
770 fractionation on two different deuterium excess definitions. *Journal of Geophysical Research:*
771 *Atmospheres*, *122*(23), 12–732.
772 Eckhardt, S., Hermansen, O., Grythe, H., Fiebig, M., Stebel, K., Cassiani, M., et al. (2013). The
773 influence of cruise ship emissions on air pollution in Svalbard - a harbinger of a more polluted
774 Arctic? *Atmospheric Chemistry and Physics*, *13*(16), 8401–8409. https://doi.org/10.5194/acp-
775 13-8401-2013
776 Galewsky, J., Steen-Larsen, H. C., Field, R. D., Worden, J., Risi, C., & Schneider, M. (2016). Stable
777 isotopes in atmospheric water vapor and applications to the hydrologic cycle: ISOTOPES IN
778 THE ATMOSPHERIC WATER CYCLE. *Reviews of Geophysics*, *54*(4), 809–865.
779 https://doi.org/10.1002/2015RG000512
780 Gjelten, H. M., Nordli, Ø., Isaksen, K., Førland, E. J., Sviashchennikov, P. N., Wyszynski, P., et al.
781 (2016). Air temperature variations and gradients along the coast and fjords of western
782 Spitsbergen. *Polar Research*, *35*(1), 29878. https://doi.org/10.3402/polar.v35.29878

783 Goosse, H., Kay, J. E., Armour, K. C., Bodas-Salcedo, A., Chepfer, H., Docquier, D., et al. (2018).
784 Quantifying climate feedbacks in polar regions. *Nature Communications*, *9*(1), 1919.
785 https://doi.org/10.1038/s41467-018-04173-0
786 Hanssen-Bauer, I., & Førland, E. (1998). Long-term trends in precipitation and temperature in the
787 Norwegian Arctic: can they be explained by changes in atmospheric circulation patterns?
788 *Climate Research*, *10*, 143–153. https://doi.org/10.3354/cr010143
789 Hao, M., Luo, Y., Lin, Y., Zhao, Z., Wang, L., & Huang, J. (2019). Contribution of atmospheric moisture
790 transport to winter Arctic warming. *International Journal of Climatology*, *39*(5), 2697–2710.
791 https://doi.org/10.1002/joc.5982
792 Hendricks, M. B., DePaolo, D. J., & Cohen, R. C. (2000). Space and time variation of δ18O and δD in
793 precipitation: Can paleotemperature be estimated from ice cores? *Global Biogeochemical*
794 *Cycles*, *14*(3), 851–861. https://doi.org/10.1029/1999GB001198
795 International Atomic Energy Agency. (2006). *Reference Sheet for International Measurement*
796 *Standards*. Retrieved from https://nucleus.iaea.org/rpst/documents/VSMOW_SLAP.pdf
797 Isaksen, K., Nordli, Ø., Førland, E. J., Łupikasza, E., Eastwood, S., & Niedźwiedź, T. (2016). Recent
798 warming on Spitsbergen-Influence of atmospheric circulation and sea ice cover. *Journal of*
799 *Geophysical Research: Atmospheres*, *121*(20), 11,913-11,931.
800 https://doi.org/10.1002/2016JD025606
801 Isaksson, E., Kohler, J., Pohjola, V., Moore, J., Igarashi, M., Karlöf, L., et al. (2005). Two ice-core δ18O
802 records from Svalbard illustrating climate and sea-ice variability over the last 400 years. *The*
803 *Holocene*, *15*(4), 501–509. https://doi.org/10.1191/0959683605hl820rp
804 Jouzel, J., Delaygue, G., Landais, A., Masson-Delmotte, V., Risi, C., & Vimeux, F. (2013). Water
805 isotopes as tools to document oceanic sources of precipitation: Water Isotopes and
806 Precipitation Origin. *Water Resources Research*, *49*(11), 7469–7486.
807 https://doi.org/10.1002/2013WR013508

808 Jouzel, Jean, & Merlivat, L. (1984). Deuterium and oxygen 18 in precipitation: Modeling of the
809 isotopic effects during snow formation. *Journal of Geophysical Research: Atmospheres*,
810 *89*(D7), 11749–11757.
811 Kopec, B. G., Lauder, A. M., Posmentier, E. S., & Feng, X. (2014). The diel cycle of water vapor in west
812 Greenland: west Greenland diel cycle of water vapor. *Journal of Geophysical Research:*
813 *Atmospheres*, *119*(15), 9386–9399. https://doi.org/10.1002/2014JD021859
814 Kopec, B. G., Feng, X., Posmentier, E. S., & Sonder, L. J. (2019). Seasonal Deuterium Excess Variations
815 of Precipitation at Summit, Greenland, and their Climatological Significance. *Journal of*
816 *Geophysical Research: Atmospheres*, *124*(1), 72–91. https://doi.org/10.1029/2018JD028750
817 Kurita, N. (2003). Relationship between the variation of isotopic ratios and the source of summer
818 precipitation in eastern Siberia. *Journal of Geophysical Research*, *108*(D11), 4339.
819 https://doi.org/10.1029/2001JD001359
820 Liu, C., & Barnes, E. A. (2015). Extreme moisture transport into the Arctic linked to Rossby wave
821 breaking: extreme moisture flux and wave breaking. *Journal of Geophysical Research:*
822 *Atmospheres*, *120*(9), 3774–3788. https://doi.org/10.1002/2014JD022796
823 Majoube, M. (1971). Fractionnement en δ18O entre la glace et la vapeur d'eau. *Journal de Chimie*
824 *Physique*, *68*, 625–636.
825 Masson-Delmotte, V., Hou, S., Ekaykin, A., Jouzel, J., Aristarain, A., Bernardo, R. T., et al. (2008). A
826 Review of Antarctic Surface Snow Isotopic Composition: Observations, Atmospheric
827 Circulation, and Isotopic Modeling. *Journal of Climate*, *21*(13), 3359–3387.
828 https://doi.org/10.1175/2007JCLI2139.1
829 Maturilli, M. (2018). High resolution radiosonde measurements from station Ny-Ålesund (2017-12).
830 PANGAEA. https://doi.org/10.1594/PANGAEA.886871
831 Maturilli, M. (2020a). Basic and other measurements of radiation at station Ny-Ålesund (2020-04).
832 PANGAEA. https://doi.org/10.1594/PANGAEA.917580

833 Maturilli, M. (2020b). High resolution radiosonde measurements from station Ny-Ålesund (2017-04
834 et seq). PANGAEA. https://doi.org/10.1594/PANGAEA.914973
835 Maturilli, M., & Ebell, K. (2018). Twenty-five years of cloud base height measurements by ceilometer
836 in Ny-Ålesund, Svalbard. *Earth System Science Data*, *10*(3), 1451–1456.
837 https://doi.org/10.5194/essd-10-1451-2018
838 Maturilli, M., & Kayser, M. (2017). Arctic warming, moisture increase and circulation changes
839 observed in the Ny-Ålesund homogenized radiosonde record. *Theoretical and Applied*
840 *Climatology*, *130*(1–2), 1–17. https://doi.org/10.1007/s00704-016-1864-0
841 Meredith, M., Sommerkorn, M., Cassota, S., Derksen, C., Ekaykin, A., Hollowed, A., et al. (2019). *IPCC*
842 *Special Report on the Ocean and Cryosphere in a Changing Climate: Chapter 3: Polar Regions*.
843 Merlivat, L., & Nief, G. (1967). Fractionnement isotopique lors des changements d'état solide-vapeur
844 et liquide-vapeur de l'eau à des températures inférieures à 0°C. *Tellus*, *19*(1), 122–127.
845 https://doi.org/10.1111/j.2153-3490.1967.tb01465.x
846 Merlivat, Liliane, & Jouzel, J. (1979). Global climatic interpretation of the deuterium-oxygen 18
847 relationship for precipitation. *Journal of Geophysical Research*, *84*(C8), 5029.
848 https://doi.org/10.1029/JC084iC08p05029
849 Naakka, T., Nygård, T., Vihma, T., Sedlar, J., & Graversen, R. (2019). Atmospheric moisture transport
850 between mid-latitudes and the Arctic: Regional, seasonal and vertical distributions.
851 *International Journal of Climatology*, *39*(6), 2862–2879. https://doi.org/10.1002/joc.5988
852 Ngan, F., Loughner, C. P., & Stein, A. (2019). The evaluation of mixing methods in HYSPLIT using
853 measurements from controlled tracer experiments. *Atmospheric Environment*, *219*, 117043.
854 Nomokonova, T., Ebell, K., Löhnert, U., Maturilli, M., & Ritter, C. (2020). The influence of water vapor
855 anomalies on clouds and their radiative effect at Ny-Ålesund. *Atmospheric*
856 *Chemistry and Physics*, *20*(8), 5157–5173. https://doi.org/10.5194/acp-20-5157-2020
857 Opel, T., Fritzsche, D., Meyer, H., Schütt, R., Weiler, K., Ruth, U., et al. (2009). 115 year ice-core data
858 from Akademii Nauk ice cap, Severnaya Zemlya: high-resolution record of Eurasian Arctic

climate change. *Journal of Glaciology*, *55*(189), 21–31. https://doi.org/10.3189/002214309788609029

Overland, J. E., & Wang, M. (2018). Arctic-midlatitude weather linkages in North America. *Polar Science*, *16*, 1–9. https://doi.org/10.1016/j.polar.2018.02.001

Papritz, L., & Sodemann, H. (2018). Characterizing the Local and Intense Water Cycle during a Cold Air Outbreak in the Nordic Seas. *Monthly Weather Review*, *146*(11), 3567–3588. https://doi.org/10.1175/MWR-D-18-0172.1

Picarro Inc. (2009). *L1102-i Analyzer User's Guide*. Sunnyvale, CA, USA: Picarro Inc., Sunnyvale, CA, USA. Retrieved from https://www.picarro.com/support/documents

Picarro Inc. (2016). *L2130-i Analyzer User's Guide*. Sunnyvale, CA, USA: Picarro Inc., Sunnyvale, CA, USA. Retrieved from https://www.picarro.com/support/documents

Rayleigh, Lord. (1902). LIX. On the distillation of binary mixtures. *The London, Edinburgh, and Dublin Philosophical Magazine and Journal of Science*, *4*(23), 521–537.

Rinke, A., Maturilli, M., Graham, R. M., Matthes, H., Handorf, D., Cohen, L., et al. (2017). Extreme cyclone events in the Arctic: Wintertime variability and trends. *Environmental Research Letters*, *12*(9), 094006. https://doi.org/10.1088/1748-9326/aa7def

Rinke, A., Segger, B., Crewell, S., Maturilli, M., Naakka, T., Nygård, T., et al. (2019). Trends of Vertically Integrated Water Vapor over the Arctic during 1979–2016: Consistent Moistening All Over? *Journal of Climate*, *32*(18), 6097–6116. https://doi.org/10.1175/JCLI-D-19-0092.1

Risi, C., Bony, S., & Vimeux, F. (2008). Influence of convective processes on the isotopic composition (δ18O and δD) of precipitation and water vapor in the tropics: 2. Physical interpretation of the amount effect. *Journal of Geophysical Research: Atmospheres*, *113*(D19).

Risi, C., Bony, S., Vimeux, F., Chong, M., & Descroix, L. (2010). Evolution of the stable water isotopic composition of the rain sampled along Sahelian squall lines. *Quarterly Journal of the Royal Meteorological Society*, *136*(S1), 227–242.

884 Risi, C., Bony, S., Vimeux, F., & Jouzel, J. (2010). Water-stable isotopes in the LMDZ4 general
885 circulation model: Model evaluation for present-day and past climates and applications to
886 climatic interpretations of tropical isotopic records. *Journal of Geophysical Research*,
887 *115*(D12), D12118. https://doi.org/10.1029/2009JD013255
888 Ritter, F., Steen-Larsen, H. C., Werner, M., Masson-Delmotte, V., Orsi, A., Behrens, M., et al. (2016).
889 Isotopic exchange on the diurnal scale between near-surface snow and lower atmospheric
890 water vapor at Kohnen station, East Antarctica. *The Cryosphere*, *10*(4), 1647–1663.
891 https://doi.org/10.5194/tc-10-1647-2016
892 Screen, J. A., & Simmonds, I. (2010). The central role of diminishing sea ice in recent Arctic
893 temperature amplification. *Nature*, *464*(7293), 1334–1337.
894 https://doi.org/10.1038/nature09051
895 Smith, R. B., & Evans, J. P. (2007). Orographic Precipitation and Water Vapor Fractionation over the
896 Southern Andes. *Journal of Hydrometeorology*, *8*(1), 3–19.
897 https://doi.org/10.1175/JHM555.1
898 Sodemann, H., Schwierz, C., & Wernli, H. (2008). Interannual variability of Greenland winter
899 precipitation sources: Lagrangian moisture diagnostic and North Atlantic Oscillation
900 influence. *Journal of Geophysical Research*, *113*(D3), D03107.
901 https://doi.org/10.1029/2007JD008503
902 Sodemann, Harald, Aemisegger, F., Pfahl, S., Bitter, M., Corsmeier, U., Feuerle, T., et al. (2017). The
903 stable isotopic composition of water vapour above Corsica during the HyMeX SOP1
904 campaign: insight into vertical mixing processes from lower-tropospheric survey flights.
905 *Atmospheric Chemistry and Physics*, *17*(9), 6125–6151.
906 Steen-Larsen, H. C., Masson-Delmotte, V., Sjolte, J., Johnsen, S. J., Vinther, B. M., Bréon, F.-M., et al.
907 (2011). Understanding the climatic signal in the water stable isotope records from the NEEM
908 shallow firn/ice cores in northwest Greenland. *Journal of Geophysical Research*, *116*(D6),
909 D06108. https://doi.org/10.1029/2010JD014311

910 Steen-Larsen, H. C., Johnsen, S. J., Masson-Delmotte, V., Stenni, B., Risi, C., Sodemann, H., et al.
911 (2013). Continuous monitoring of summer surface water vapor isotopic composition above
912 the Greenland Ice Sheet. *Atmospheric Chemistry and Physics*, *13*(9), 4815–4828.
913 https://doi.org/10.5194/acp-13-4815-2013
914 Steen-Larsen, H. C., Masson-Delmotte, V., Hirabayashi, M., Winkler, R., Satow, K., Prié, F., et al.
915 (2014). What controls the isotopic composition of Greenland surface snow? *Climate of the*
916 *Past*, *10*(1), 377–392. https://doi.org/10.5194/cp-10-377-2014
917 Steen-Larsen, H. C., Sveinbjörnsdottir, A. E., Jonsson, Th., Ritter, F., Bonne, J.-L., Masson-Delmotte,
918 V., et al. (2015). Moisture sources and synoptic to seasonal variability of North Atlantic water
919 vapor isotopic composition: north Atlantic water vapor isotopes. *Journal of Geophysical*
920 *Research: Atmospheres*, *120*(12), 5757–5774. https://doi.org/10.1002/2015JD023234
921 Steen-Larsen, H. C., Risi, C., Werner, M., Yoshimura, K., & Masson-Delmotte, V. (2017). Evaluating the
922 skills of isotope-enabled general circulation models against in situ atmospheric water vapor
923 isotope observations: Evaluating Isotope-Enabled GCMs. *Journal of Geophysical Research:*
924 *Atmospheres*, *122*(1), 246–263. https://doi.org/10.1002/2016JD025443
925 Stein, A. F., Draxler, R. R., Rolph, G. D., Stunder, B. J. B., Cohen, M. D., & Ngan, F. (2015). NOAA's
926 HYSPLIT Atmospheric Transport and Dispersion Modeling System. *Bulletin of the American*
927 *Meteorological Society*, *96*(12), 2059–2077. https://doi.org/10.1175/BAMS-D-14-00110.1
928 Stern, L. A., & Blisniuk, P. M. (2002). Stable isotope composition of precipitation across the southern
929 Patagonian Andes: stable isotope composition of precipitation. *Journal of Geophysical*
930 *Research: Atmospheres*, *107*(D23), ACL 3-1-ACL 3-14. https://doi.org/10.1029/2002JD002509
931 Stohl, A., Forster, C., Frank, A., Seibert, P., & Wotawa, G. (2005). The Lagrangian particle dispersion
932 model FLEXPART version 6.2. *Atmos. Chem. Phys.*, 14.
933 Touzeau, A., Landais, A., Stenni, B., Uemura, R., Fukui, K., Fujita, S., et al. (2016). Acquisition of
934 isotopic composition for surface snow in East Antarctica and the links to climatic parameters.
935 *The Cryosphere*, 17.

936 Tremoy, G., Vimeux, F., Cattani, O., Mayaki, S., Souley, I., & Favreau, G. (2011). Measurements of
937 water vapor isotope ratios with wavelength-scanned cavity ring-down spectroscopy
938 technology: new insights and important caveats for deuterium excess measurements in
939 tropical areas in comparison with isotope-ratio mass spectrometry: Measuring tropical water
940 vapor isotope ratios using WS-CRDS. *Rapid Communications in Mass Spectrometry*, *25*(23),
941 3469–3480. https://doi.org/10.1002/rcm.5252
942 Uemura, R., Masson-Delmotte, V., Jouzel, J., Landais, A., Motoyama, H., & Stenni, B. (2012). Ranges
943 of moisture-source temperature estimated from Antarctic ice cores stable isotope records
944 over glacial–interglacial cycles. *Climate of the Past*, *8*(3), 1109–1125.
945 https://doi.org/10.5194/cp-8-1109-2012
946 Vázquez, M., Nieto, R., Drumond, A., & Gimeno, L. (2016). Moisture transport into the Arctic: Source-
947 receptor relationships and the roles of atmospheric circulation and evaporation. *Journal of*
948 *Geophysical Research: Atmospheres*, *121*(22), 13,493-13,509.
949 https://doi.org/10.1002/2016JD025400
950 Walsh, J. E., Fetterer, F., Scott stewart, J., & Chapman, W. L. (2017). A database for depicting Arctic
951 sea ice variations back to 1850. *Geographical Review*, *107*(1), 89–107.
952 https://doi.org/10.1111/j.1931-0846.2016.12195.x
953 Werner, M., Langebroek, P. M., Carlsen, T., Herold, M., & Lohmann, G. (2011). Stable water isotopes
954 in the ECHAM5 general circulation model: Toward high-resolution isotope modeling on a
955 global scale. *Journal of Geophysical Research*, *116*(D15), D15109.
956 https://doi.org/10.1029/2011JD015681
957 Woods, C., Caballero, R., & Svensson, G. (2013). Large-scale circulation associated with moisture
958 intrusions into the Arctic during winter. *Geophysical Research Letters*, *40*(17), 4717–4721.
959 https://doi.org/10.1002/grl.50912
960 Zhang, X., Walsh, J. E., & Zhang, J. (2004). Climatology and Interannual Variability of Arctic Cyclone
961 Activity: 1948–2002. *JOURNAL OF CLIMATE*, *17*, 19.

962

963